ACS APPLIED BIO MATERIALS

www.acsabm.org Article

Electrochemical DNA Biosensors Based on the Intrinsic Topological Insulator $BiSbTeSe_2$ for Potential Application in HIV Determination

Yujiu Jiang, Shanshan Li, Peng Zhu, Jinge Zhao, Xiaolu Xiong, Yetong Wu, Xu Zhang, Yongkai Li, Tinglu Song, Wende Xiao, Zhiwei Wang,* and Junfeng Han*

Cite This: *ACS Appl. Bio Mater.* 2022, 5, 1084−1091 Read Online

ACCESS | Metrics & More | Article Recommendations | Supporting Information

ABSTRACT: In this work, we reported a sensitive, label-free electrochemical biosensor based on the intrinsic topological insulator (TI) $BiSbTeSe_2$ for potential application in the determination of the HIV gene. With strong spin−obit coupling, TIs could have robust surface states with low electronic noise, which might be beneficial for the stable and sensitive electron transport between the electrode and electrolyte interface. Under optimized conditions of the biosensors using $BiSbTeSe_2$, the differential pulse voltammetry (DPV) peak currents showed a linear relationship with the logarithm of target DNA concentrations ranging from 1.0×10^{-13} to 1.0×10^{-7} M, with a detection limit of 1.07×10^{-15} M. The sensing assay also displayed good selectivity and stability after storage at 4 °C for 7 days. This work provides an effective way to develop biosensors with topological materials, which have a potential application in the clinical determination and monitoring field.

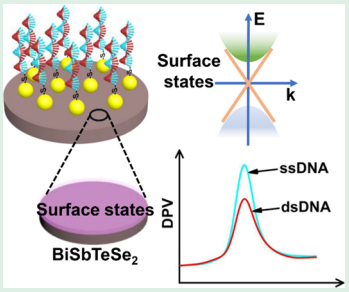

KEYWORDS: *label-free, topological insulator, $BiSbTeSe_2$, electrochemical biosensor, differential pulse voltammetry*

1. INTRODUCTION

Various viruses with high infectivity have threatened human health in history; e.g., the human immunodeficiency virus-1 (HIV-1) is the most common reason of AIDS infection.[1−3] Direct detection of HIV-1 DNA is quite significant for the early diagnosis of AIDS infection, which can efficiently identify the infected individuals, expand treatment service, and protect the healthy population. Therefore, it is necessary to develop a sensitive, selective, and accurately quantitative method to determine the DNA series for infection diagnosis. Various DNA diagnosis methods have been developed, including polymerase chain reaction (PCR),[4−7] optics,[8−10] electrochemistry,[11−14] electrogenerated chemiluminescence (ECL),[15−17] and electrochemical biosensors.[18−22] Among various methods for biomolecule detection, electrochemical biosensors have many advantages, such as easy and fast operation, high sensitivity, and simple data analysis.[23−27] To develop high-performance electrochemical biosensors, it is essential to use electrodes with high electron conductivity to promote interfacial charge transfer and strong stability to provide reliable results. Recently, topological insulators (TIs) have been used as electrochemical electrode materials to make a sensitive DNA detector.[28] TI is a kind of new phase of quantum matter with an insulator bulk and conductive surface/edge states. As they are protected by time-reversal symmetry, the TIs can have robust surface/edge states that are immune to small time-reversal perturbations such as backscattering, crystal disorders, and nonmagnetic impurities,[29−32] leading to low electronic noise,[33−35] which may be beneficial for the stable and sensitive electron transport between the electrode and electrolyte interface.[36,37] Such surface properties can be employed to develop a high signal-to-noise ratio electrochemical biosensor with low detection limits.

The M_2X_3 (M = Bi, Sb; X = Te, Se) family serves as a kind of typical topological insulators with a large bulk band gap and gapless surface states, which can theoretically form a dissipationless electron conduction channel at room temperature.[38,39] Because of its biocompatibility, Bi_2Se_3 has been employed for clinical practices like biomarker detection and diagnosis.[40,41] Thus, the topological material Bi_2Se_3 has good environmental friendliness, stability, and biocompatibility, which make it a potential candidate immobilized substrate for biomolecules. However, most of the papers reported TIs as nanosheets or nanoparticles,[42,43] whose repeatability and stability can be difficult to control due to large amounts of defects and grain boundaries. On the other hand, due to the high doping of Bi_2Se_3 or Bi_2Te_3, it is difficult to obtain an intrinsic M_2X_3 topological insulator with the Fermi level located in the band gap for biosensor applications and related physical mechanisms.[44,45] Therefore, it will attract great interest to develop a biosensor based on an intrinsic topological insulator crystal and study its working mechanism. The Sb-doped Bi_2Se_3 or Bi_2Te_3 single crystals were reported to

Received: November 10, 2021
Accepted: February 1, 2022
Published: February 14, 2022

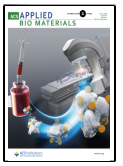

https://doi.org/10.1021/acsabm.1c01153
ACS Appl. Bio Mater. 2022, 5, 1084−1091

Scheme 1. Schematic Diagram of the Preparation Process of the Electrochemical DNA Biosensor Based on $BiSbTeSe_2$

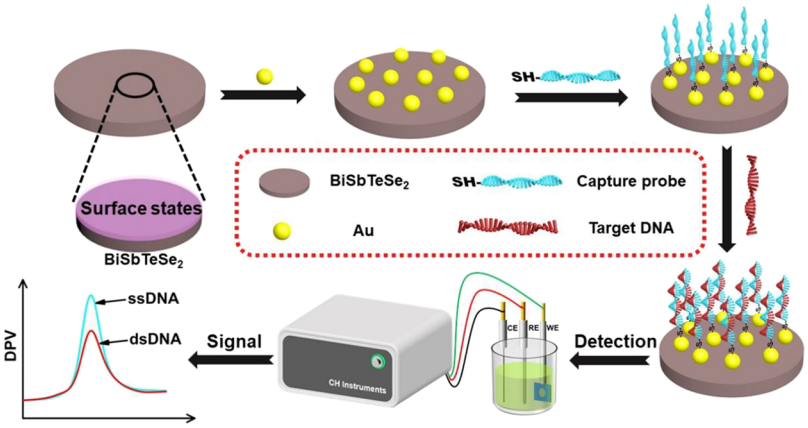

be a kind of intrinsic topological insulators with Fermi levels located at the band gap. Such materials can be suitable for investigating the quantum transport properties and carrier dynamics.[46−49]

In this study, a high-quality intrinsic topological insulator, the $BiSbTeSe_2$ single crystal, was grown by the melting method. The high quality could avoid the harmful effects of defects and grain boundaries, while the intrinsic property could be beneficial for exhibiting the contribution of surface states in the device. Using the above crystal as the work electrode, a DNA biosensor was designed and fabricated with high sensitivity and selectivity for the determination of the HIV gene. Differential pulse voltammetry (DPV) was carried out to investigate the sensitivity, selectivity, and stability of the biosensors. The results indicate that $BiSbTeSe_2$ based biosensors can achieve a detection limit of 1.07×10^{-15} M. It also has a wide linear response range, high selectivity, and excellent stability, which make the topological insulator a good candidate for a biosensor electrode material.

The work principle of the DNA biosensor preparation is described in Scheme 1. Initially, a mm-scale thin layer of $BiSbTeSe_2$ single crystal was exfoliated by a stick and insulator tape. The schematic diagram of the surface states of $BiSbTeSe_2$ is shown in Figure S1. Then the gold particles (AuNPs) were sputtered on the surface of the $BiSbTeSe_2$ to improve the connection between $BiSbTeSe_2$ and DNA. Subsequently, the thiol-modified single-stranded DNA capture probe was immobilized on the AuNPs/$BiSbTeSe_2$ with a Au−S bond. Thus, a DNA biosensor based on the topological insulator was constructed to determine the target DNA. By using the electrochemical impedance spectroscopy (EIS) or differential pulse voltammetry (DPV) method, it is possible to identify whether the probe DNA could capture the right target DNA selectively or not. Thus, a sensitive biosensor was considered to be successfully constructed for detecting target DNA like the HIV gene, which had a potential application for disease determination and clinical analysis.

2. EXPERIMENTAL SECTION

2.1. Oligonucleotides and Reagents. The phosphate buffer saline (PBS, pH 7.4) was purchased from Biomed (Beijing, China). The Tris-EDTA (TE) buffer solution (10 mM Tris−HCl, 1.0 mM EDTA, pH = 8.0) was purchased from Solarbio Bioscience & Technology Co., Ltd. (Beijing, China). Potassium hexacyanoferrate-(III) ($K_3[Fe(CN)_6]$, ≥99.5%) and potassium hexacyanoferrate(II) ($K_4[Fe(CN)_6]$, ≥99%) were purchased from Macklin. All oligonucleotides used in the experiment were synthesized by Sangon Biotech Inc. (Shanghai, China). Ultrapure water (resistivity of 18.2 MΩ·cm) was used in all of the experiments. Bi (99.997%, Alfa Aesar), Sb, Se, and Te chunks (99.999%, Alfa Aesar) were used to grow the $BiSbTeSe_2$ single crystal. All chemicals used in this work were of analytical reagent grade. The stock solution of DNA was prepared in a TE buffer solution (10 mM Tris−HCl, 1.0 mM EDTA, pH = 8.0). All solutions and oligonucleotide were kept at 4 °C in a refrigerator.

The DNA oligonucleotides of the HIV gene were synthesized by Shanghai Sangon Bioengineering Limited Company (China), and the base sequences are shown below:

Single-stranded DNA (ssDNA): 5′-SH-$(CH_2)_6$-AGT CAG TGT GGA AAA TCT CTA GC-3′

Target complementary DNA (tDNA): 5′-GCT AGA GAT TTT CCA CAC TGA CT-3′

One-base mismatched DNA (Mis1): 5′-GCT AGA GAT TTT CAA CAC TGA CT-3′

Two-base mismatched DNA (Mis2): 5′-GCT CGA GAT TTT CAA CAC TGA CT-3′

Three-base mismatched DNA (Mis3): 5′-GCT CGA GAT TTT CAA CAC GGA CT-3′

Noncomplementary DNA (Nc): 5′-TAG CCG AGC GGC TTC AGT GAC AG-3′

2.2. Instruments. The $BiSbTeSe_2$ single crystal was grown by using a muffle furnace (KSL-1200X). The surface morphologies were characterized by a scanning electron microscope (SEM, ZEISS Gemini SEM 360). The high-resolution high-angle annular dark field scanning transmission electron microscope (HAADF-STEM) image was obtained under a Cs-corrected STEM (ThermoFisher, Themis Z) operated at 200 kV with a convergence semi-angle of 25 mrad. The crystalline phase of $BiSbSeTe_2$ was featured by X-ray diffraction (XRD, Bruker D8 Advance). The surface chemical composition was analyzed by an X-ray photoelectron spectroscope (XPS, PHI Quantera II) with an Al Kα monochrome X-ray ($h\nu$=1486.6 eV) source. All the binding energies of the XPS spectra were calibrated by using the C 1s peak (284.8 eV). The surface roughness was measured by using an atomic force microscope (AFM, Bruker Multimode 8) with tapping mode under ambient conditions. The electrical properties were measured by using a physical property measurement system (PPMS, Quantum Design Dynacool-14). An integrated ion sputtering/thermal evaporation coating system (Quorum, Q150R ES) was used to provide gold particles.

2.3. Preparation of $BiSbTeSe_2$. High-quality single crystals of $BiSbTeSe_2$ were grown using pretreated Bi, Sb, Se, and Te chunks (99.999%, Alfa Aesar) as starting materials. To obtain these crystals, stoichiometric mixtures of elements were melted at 850 °C for 48 h in an evacuated sealed quartz tube accompanied with shaking of the tube followed by slow cooling at a rate of 5 °C/h to 550 °C. Shiny plates could be cut out from the obtained crystals.

https://doi.org/10.1021/acsabm.1c01153
ACS Appl. Bio Mater. 2022, 5, 1084−1091

2.4. Preparation of the AuNPs/BiSbTeSe$_2$ Electrode. A mm-scale thin layer of the BiSbTeSe$_2$ single crystal was exfoliated by a stick and insulator tape. Then the sputtering current of the integrated ion sputtering/thermal evaporation coating system was set as 23 mA and sputtering time was set as 10 s. Finally, the obtained thin layer of BiSbTeSe$_2$ single crystal was placed on the integrated ion sputtering/thermal evaporation coating system to prepare the AuNPs/BiSbTeSe$_2$ electrode.

2.5. Immobilization and Hybridization of DNA. The TE (10 μL, pH = 8.0) buffer solution containing ssDNA probes (1.0×10^{-7} M) was pipetted onto the AuNPs/BiSbTeSe$_2$ electrode, incubated overnight at 4 °C, and rinsed with the TE (pH = 8.0) buffer solution to remove the unimmobilized ssDNA. Thus, the probe-captured electrode was denoted as the ssDNA/AuNPs/BiSbTeSe$_2$ electrode. Subsequently, 10 μL of the TE (pH = 8.0) buffer solution containing tDNA was pipetted onto the probe-modified electrode. After incubation at 37 °C for 2 h, the TE (pH = 8.0) buffer solution was used to rinse the electrode to remove the unhybridized tDNA. The hybridization process of the probe modified electrode with Mis1, Mis2, Mis3, and Nc was the same as the above steps.

2.6. Electrochemical Measurements. All electrochemical experiments were carried out using a CHI 650E electrochemical workstation (Chenhua Instruments Co., Shanghai, China) at room temperature by using a conventional three-electrode system comprising a platinum wire auxiliary electrode, KCl-saturated Ag/AgCl reference electrode, and BiSbTeSe$_2$ working electrode. The involved electrochemical analysis methods included differential pulse voltammetry (DPV), cyclic voltammetry (CV), and electrochemical impedance spectroscopy (EIS). The supporting electrolyte solution was 0.1 M PBS (pH = 7.4) containing 0.1 M KCl and 10 mM $[Fe(CN)_6]^{3-/4-}$. Differential pulse voltammetry (DPV) signals were measured by using parameters as follows: pulse step, 4 mV; pulse amplitude, 50 mV; pulse width, 0.05 s; and pulse period, 0.5 s. A cyclic voltammetry (CV) scan from −0.2 to 0.6 V was performed at a scan rate of 50 mV/s, and electrochemical impedance spectroscopy (EIS) was recorded with the frequency ranging from 0.1 Hz to 100 kHz at an amplitude of 5 mV.

3. RESULTS AND DISCUSSION

3.1. Characterization of the BiSbTeSe$_2$ and AuNPs/BiSbTeSe$_2$. Figure 1A shows a SEM image of the BiSbTeSe$_2$.

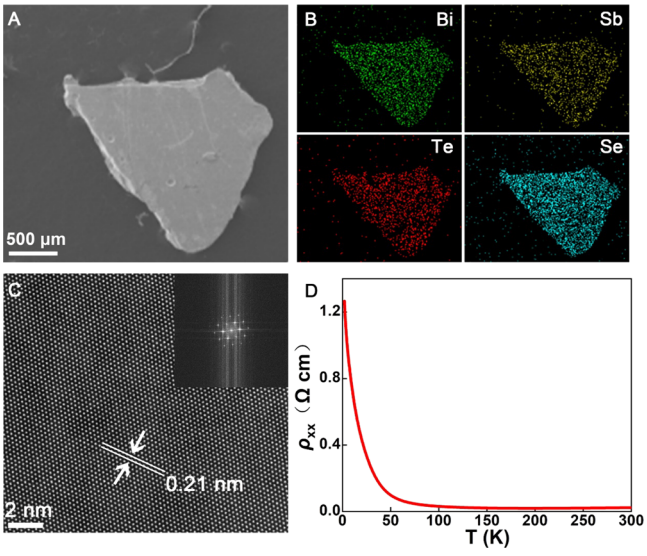

Figure 1. (A) SEM image of the BiSbTeSe$_2$. (B) Elemental mapping of the BiSbTeSe$_2$, including Bi, Sb, Te, and Se. (C) STEM image of the BiSbTeSe$_2$. Inset is the FFT image of panel C. (D) Temperature-dependent ρ_{xx} of the BiSbTeSe$_2$.

Elemental mapping of the BiSbTeSe$_2$ (Figure 1B) exhibits that Bi, Sb, Te, and Se were all uniformly distributed throughout the BiSbTeSe$_2$ crystal. Several distinguished diffraction peaks, which correspond to (003), (006), (009), (0012), (0015), (0018), and (0021), confirm the pure phase of BiSbTeSe$_2$ (Figure S2). The small sheets were exfoliated from the BiSbTeSe$_2$ single crystal for the observation of the scanning transmission electron microscope (STEM). The high-resolution STEM image (Figure 1C) and the FFT inset (top right) reveal that the prepared BiSbTeSe$_2$ crystal has a quite high quality without any defect. The crystal structure of BiSbTeSe$_2$ is shown in Figure S3. Electrical measurements were performed on BiSbTeSe$_2$ single crystals to identify their semiconductor properties. Figure 1D shows the temperature-dependent longitudinal resistivity ρ_{xx}. With decreasing temperature, the samples roughly undergo an increase in ρ_{xx} at the temperature range of 2−300 K. The curve of $\rho(T)$ can be explained by the thermal activation model, which indicates an active energy of 10 meV. Such temperature-dependent behavior demonstrates the intrinsic electric properties of BiSbTeSe$_2$ crystals.

The surface chemical compositions of the AuNPs/BiSbTeSe$_2$ were evaluated by X-ray photoelectron spectroscopy (XPS) measurement. Figure 2A shows the XPS survey scan

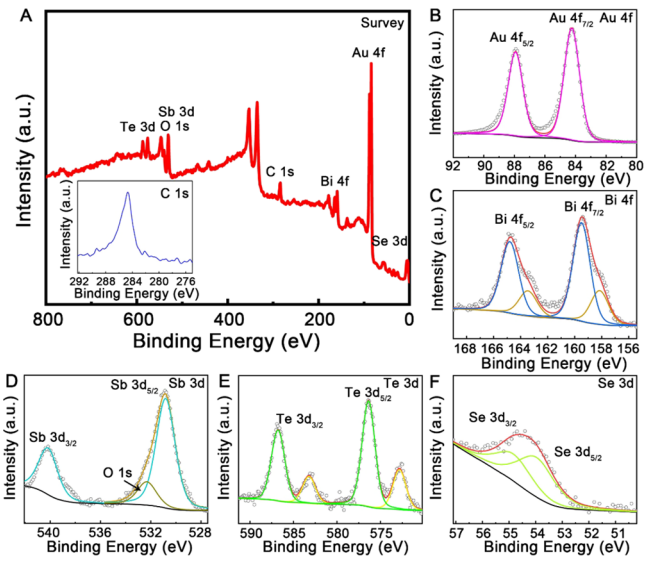

Figure 2. XPS spectra of the AuNPs/BiSbTeSe$_2$ surface: (A) survey scan spectrum (inset: spectra of C 1s); core levels of (B) Au 4f, (C) Bi 4f, (D) Sb 3d, (E) Te 3d, and (F) Se 3d.

including the elements Au, Bi, Sb, Te, and Se, and the inset is the core level of C 1s with peak correction to 284.8 eV. In Figure 2B, Au 4f$_{7/2}$ and Au 4f$_{5/2}$ were observed at 84.2 and 87.9 eV, respectively, suggesting a Au^0 state existing on the obtained AuNPs/BiSbTeSe$_2$.[50,51] In Figure 2C, Bi 4f$_{7/2}$ and Bi 4f$_{5/2}$ are split into two components and located at 158.2 and 159.5 eV and 163.5 and 164.8 eV, respectively. The Bi component with higher binding energy might be related to some possible oxides. Anyway, such oxides can only exist on the surface of the sample. By slightly sputtering with Ar ion, those oxides completely disappeared as shown in Figure S4. In Figure 2D, the peaks located at 530.8 and 540.2 eV are attributed to Sb 3d$_{5/2}$ and Sb 3d$_{3/2}$, respectively. The peak intensity of Sb 3d$_{5/2}$ is obviously larger than that of Sb 3d$_{3/2}$,

https://doi.org/10.1021/acsabm.1c01153
ACS Appl. Bio Mater. 2022, 5, 1084−1091

which is due to the overlap with the O 1s peak (532.3 eV). The peaks of Te $3d_{5/2}$ and Te $3d_{3/2}$ are located at 572.8 and 576.4 eV and 583.2 and 586.8 eV (Figure 2E), respectively. The Te components with higher binding energy may also correspond to oxides. Figure 2F illustrates the core levels of Se with a broad peak at 54.4 eV that belongs to the Se 3d level and can be further deconvoluted into two peaks: 54.0 eV for $3d_{5/2}$ and 54.8 eV for $3d_{3/2}$, respectively. All these results demonstrate the successful preparation of AuNPs/$BiSbTeSe_2$.

3.2. Electrochemical Biosensing Platform. The surface modification process of the working electrode was characterized by an atomic force microscope (AFM). As shown in Figure 3A, we could find that the surface of the $BiSbTeSe_2$

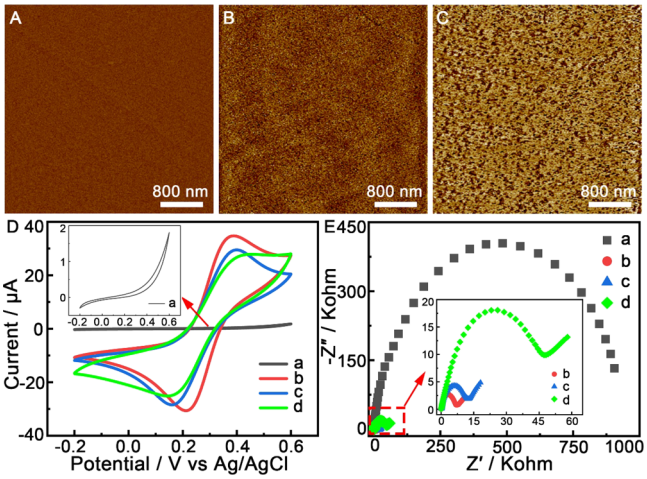

Figure 3. AFM images and electrochemical performance for the changes of interfacial properties of each immobilization step: (A) pure $BiSbTeSe_2$, (B) depositing gold on the surface of the $BiSbTeSe_2$ sheet, and (C) ssDNA modified electrode. The CV (D) and EIS (E) measurements of the modified electrodes in 0.1 M PBS (pH = 7.4) contained 0.1 M KCl and 10 mM $[Fe(CN)_6]^{3-/4-}$: (a) $BiSbTeSe_2$, (b) AuNPs/$BiSbTeSe_2$, (c) ssDNA/AuNPs/$BiSbTeSe_2$, and (d) tDNA/ssDNA/AuNPs/$BiSbTeSe_2$. The target complementary DNA concentration was 1.0×10^{-8} M.

electrode is smooth with a surface mean roughness (Ra) of 0.075 nm and a surface root mean square roughness (Rq) of 0.094 nm. After gold nanoparticles are sputtered on the surface of the $BiSbTeSe_2$ electrode (Figure 3B), the electrode surface becomes rough with Ra of 0.32 nm and Rq of 0.41 nm. The actual size of the gold particles is obtained by the SEM image (Figure S5). In the presence of ssDNA (Figure 3C), single-stranded DNA is self-assembled to the electrode surface via the formation of the Au−S bond. Figure S6 shows the three-dimensional height maps of the modified electrodes. As a result, a dense and towering morphology of the electrode surface is observed with Ra of 0.75 nm and Rq of 0.92 nm.

To investigate the surface properties of modified electrode, cyclic voltammetry (CV) and electrochemical impedance spectroscopy (EIS) were used to probe the features of surface-modified electrodes. Figure 3D shows the CV curves of various modified electrodes in PBS (pH = 7.4) containing 10 mM $[Fe(CN)_6]^{3-/4-}$ and 0.1 M KCl. The CV curve of the $BiSbTeSe_2$ electrode (curve a) shows small redox peak current. However, the CV curve of the AuNPs/$BiSbTeSe_2$ electrode (curve b) displays a pair of distinct redox peaks, illustrating the fast electron transfer of $[Fe(CN)_6]^{3-/4-}$ on the modified electrode surface. After the single-stranded DNA is immobilized, the peak current of $[Fe(CN)_6]^{3-/4-}$ at the ssDNA/AuNPs/$BiSbTeSe_2$ electrode (curve c) becomes lower than that of the AuNPs/$BiSbTeSe_2$ electrode (curve b). The distance between the oxidation and reduction peaks increases. As the negative charges of phosphoric acid groups on the single-stranded DNA restrict the diffusion of electronegative $[Fe(CN)_6]^{3-/4-}$ from the electrolyte toward the modified electrode surface, the decreased peak current reveals that the single-stranded DNA is successfully immobilized on the surface of AuNPs/$BiSbTeSe_2$ by Au−S bonds. Then, with the modification of MCH, the peak current decreases slightly by about 2.8% in the DPV curve (Figure S7). When the single-stranded DNA is hybridized with the target complementary DNA, the increased negative charges on the surface of the working electrode further attenuate the redox current (curve d).

EIS is a powerful and helpful method for evaluating the electrode interface feature modification. The corresponding Nyquist plots are illustrated in Figure 3E. All EIS tests were carried out under an open-circuit potential. A classic Randles equivalent circuit was used to fit the semicircle features of Nyquist plots. The charge-transfer resistance (R_{ct}) was extracted from the fitting results, which reveal the surface characteristics of the modified electrode. The $BiSbTeSe_2$ electrode (curve a) displays an electron transfer resistance (R_{ct}) of about 940 kΩ. The AuNPs/$BiSbTeSe_2$ electrode (curve b) shows an electron transfer resistance (R_{ct}) of about 6.64 kΩ, which confirms the good electron transfer performance with gold nanoparticles. However, the ssDNA/AuNPs/$BiSbTeSe_2$ electrode (curve c) has a quite high R_{ct} value of 12.2 kΩ compared to the AuNPs/$BiSbTeSe_2$ electrode, manifesting that ssDNA successfully self-assembled onto the surface of the AuNPs/$BiSbTeSe_2$ electrode via Au−S binding. The significant increase of R_{ct} is due to the phosphate backbone of the self-assembled ssDNA with negative charges, which produces an electrostatic repulsion force to anionic $[Fe(CN)_6]^{3-/4-}$ and prevents the diffusion of $[Fe(CN)_6]^{3-/4-}$ toward the surface of the electrode. Subsequently, in the presence of the target complementary DNA, the R_{ct} of the tDNA/ssDNA/AuNPs/$BiSbTeSe_2$ electrode is further increased to 55.2 kΩ (curve d). The increased R_{ct} is caused by the higher accumulation of negative charges on the electrode surface with the formation of the double-stranded DNA, which further restricts the diffusion of $[Fe(CN)_6]^{3-/4-}$ onto the electrode surface. CV and EIS data are consistent with each other. All these results demonstrate that the DNA biosensor has been successfully constructed according to Scheme 1.

3.3. Analytical Performance of the Electrochemical DNA Biosensor. Under the optimal experimental conditions (Figure S8), the relationship between the DPV and the concentration of target complementary DNA is shown in Figure 4. The DPV peak currents decrease with the increasing concentration of target DNA (Figure 4A). The plot of the DPV peak current vs the logarithm of target DNA concentration shows a linear relationship in the detected range from 1.0×10^{-13} to 1.0×10^{-7} M, and the corresponding linear calibration equation is $i_p = -3.80 - 3.03 \times \lg C$ (i_p is the peak current (μA) and C is the concentration of the target complementary DNA (mol/L)) and the linear correlation coefficient $R^2 = 0.984$ (Figure 4B). The low detection limit of this method is calculated to be 1.07×10^{-15} M according to the 3σ rule. Compared with other reported electrochemical DNA biosensors (Table 1), the

https://doi.org/10.1021/acsabm.1c01153
ACS Appl. Bio Mater. 2022, 5, 1084−1091

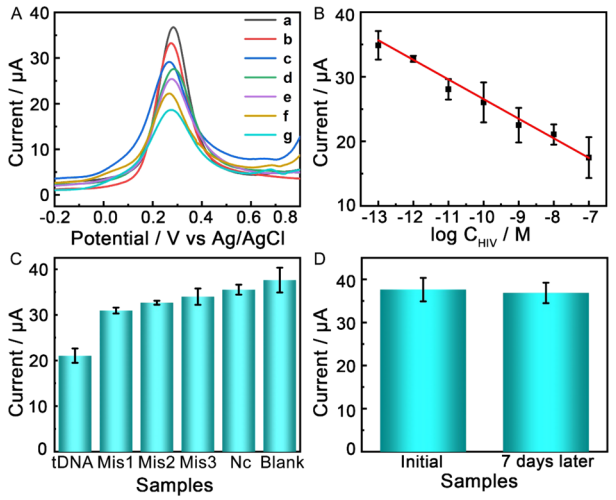

Figure 4. (A) DPV curves after hybridization increased with the increase of tDNA concentration (from a to g): 1.0×10^{-13}, 1.0×10^{-12}, 1.0×10^{-11}, 1.0×10^{-10}, 1.0×10^{-9}, 1.0×10^{-8}, and 1.0×10^{-7} M. (B) Plot of DPV peak current vs logarithm of target complementary DNA concentration. The error bars indicate the standard deviation of each concentration in three samples with the same parameters. (C) Selectivity test results of the ssDNA/AuNPs/$BiSbTeSe_2$ electrochemical DNA sensor. Histogram of the corresponding DPV peak current values of the proposed biosensor in selectivity for the target complementary DNA, one-base mismatched DNA, two-base mismatched DNA, three-base mismatched DNA, noncomplementary DNA, and blank. The concentration of each sequences was 1.0×10^{-8} M. (D) Stability test results of the ssDNA/AuNPs/$BiSbTeSe_2$ electrochemical DNA sensor with 0.1 μM single-stranded DNA after storing for 7 days at 4 °C.

Table 1. Comparison of Linear Ranges and Detection Limits of Various Reported Electrochemical Biosensors[a]

modified electrode	detection technique	linear range (M)	detection limit (M)	ref
rGO-Au/GS	DPV	1.0×10^{-9}–1.383×10^{-5}	1.0×10^{-9}	52
Ni–Au composite/CNT/PVA	DPV	1.0×10^{-8}–1.0×10^{-6}	1.3×10^{-10}	53
AuNPs/rGO	EIS	1.0×10^{-8}–2.0×10^{-5}	1.8×10^{-10}	54
GE	SWV	2.0×10^{-9}–4.0×10^{-6}	2.0×10^{-9}	55
GE	ECL	1.0×10^{-13}–1.0×10^{-6}	3.0×10^{-14}	56
Au NPs/SnO_2/ITO	PEC	5.0×10^{-15}–5.0×10^{-7}	1.38×10^{-15}	57
AuNPs/$BiSbTeSe_2$	DPV	1.0×10^{-13}–1.0×10^{-7}	1.07×10^{-15}	this work

[a]GS: graphite sheet; rGO: reduced graphene oxide; DPV: differential pulse voltammetry; CNT: carbon nanotubes; PVA: polyvinyl alcohol; EIS: electrochemical impedance spectroscopy; SWV: square wave voltammetry; GE: gold electrode; ECL: electrochemiluminescence; ITO: indium tin oxide; PEC: photoelectrochemical.

proposed biosensor has a wide linear range and relatively low detection limit. Moreover, this assay of preparing DNA biosensors is label-free. Figure 4C displays the DPV peak currents of the ssDNA/AuNPs/$BiSbTeSe_2$ before (blank) and after hybridization with the one-base mismatched DNA (Mis1), two-base mismatched DNA (Mis2), three-base mismatched DNA (Mis3), noncomplementary DNA (Nc), and target complementary DNA (tDNA). Compared to that from the original ssDNA, the currents measured on Nc and Mis3 decrease slightly by about 5.6 and 9.7%, respectively. The DPV currents decrease by about 13.2% on Mis2 and 17.8% on Mis1, respectively. As a contrast, the DPV peak current of the tDNA decreased by about 44.03%. These DPV signals indicate that the method has excellent selectivity and can distinguish between complementary sequences and different DNA sequences. For stability testing, the electrochemical DNA biosensors were stored at 4 °C for 7 days. Afterward, the current response was very stable with only a slight signal degradation (about 2.1%, shown in Figure 4D), indicating the excellent stability of the TI based DNA biosensor in this work. What's more, the reproducibility was monitored by detecting a tDNA of 1.0×10^{-8} M with six different ssDNA/AuNPs/$BiSbTeSe_2$ electrodes. The relative standard deviation (R.S.D.) was estimated to be 1.6% (Figure S9). From Figure S10, it could be seen that the DNA sensor had high selectivity in the real sample.

In one word, the above results demonstrate that the biosensors based on $BiSbTeSe_2$ are suitable for the quantitative determination of target complementary DNA concentration with high sensitivity, selectivity and stability.

4. CONCLUSIONS

In conclusion, we developed a label-free electrochemical DNA biosensor based on the intrinsic topological insulator $BiSbTeSe_2$ for HIV gene determination. The robust surface states of $BiSbTeSe_2$ may enhance the stable and sensitive electron transport between the electrode and electrolyte interface. As a result, the biosensors based on $BiSbTeSe_2$ exhibited a detection limit of 1.07×10^{-15} M, with a wide linear dynamic range from 1.0×10^{-13} to 1.0×10^{-7} M. Additionally, the biosensors showed good selectivity by distinguishing different mismatched DNA strands. Meanwhile, they also demonstrated a good stability after 1 week storage. This work offers a new path to develop sensitive biosensors based on topological insulators for the rapid and effective detection of target DNA sequence.

■ ASSOCIATED CONTENT

Supporting Information

The Supporting Information is available free of charge at https://pubs.acs.org/doi/10.1021/acsabm.1c01153.

Detailed experimental methods and supplementary figures (PDF)

■ AUTHOR INFORMATION

Corresponding Authors

Zhiwei Wang – *Centre for Quantum Physics, Key Laboratory of Advanced Optoelectronic Quantum Architecture and Measurement (MOE), School of Physics and Beijing Key Lab of Nanophotonics and Ultrafine Optoelectronic Systems, School of Physics, Beijing Institute of Technology, Beijing 100081, China; Yangtze Delta Region Academy of Beijing Institute of Technology, Jiaxing 314019, China;* Email: zhiweiwang@bit.edu.cn

Junfeng Han – *Centre for Quantum Physics, Key Laboratory of Advanced Optoelectronic Quantum Architecture and Measurement (MOE), School of Physics and Beijing Key Lab of Nanophotonics and Ultrafine Optoelectronic Systems, School of Physics, Beijing Institute of Technology, Beijing 100081, China; Yangtze Delta Region Academy of Beijing*

https://doi.org/10.1021/acsabm.1c01153
ACS Appl. Bio Mater. 2022, 5, 1084–1091

Institute of Technology, Jiaxing 314019, China; orcid.org/0000-0002-8671-966X; Email: pkuhjf@bit.edu.cn

Authors

Yujiu Jiang − *Centre for Quantum Physics, Key Laboratory of Advanced Optoelectronic Quantum Architecture and Measurement (MOE), School of Physics and Beijing Key Lab of Nanophotonics and Ultrafine Optoelectronic Systems, School of Physics, Beijing Institute of Technology, Beijing 100081, China; Yangtze Delta Region Academy of Beijing Institute of Technology, Jiaxing 314019, China*

Shanshan Li − *Department of Rheumatology, China-Japan Friendship Hospital, 100029 Beijing, China*

Peng Zhu − *Centre for Quantum Physics, Key Laboratory of Advanced Optoelectronic Quantum Architecture and Measurement (MOE), School of Physics and Beijing Key Lab of Nanophotonics and Ultrafine Optoelectronic Systems, School of Physics, Beijing Institute of Technology, Beijing 100081, China; Yangtze Delta Region Academy of Beijing Institute of Technology, Jiaxing 314019, China*

Jinge Zhao − *Key Laboratory of Medical Molecule Science and Pharmaceutics Engineering, Ministry of Industry and Information Technology, School of Chemistry and Chemical Engineering, Beijing Institute of Technology, Beijing 100081, China*

Xiaolu Xiong − *Centre for Quantum Physics, Key Laboratory of Advanced Optoelectronic Quantum Architecture and Measurement (MOE), School of Physics and Beijing Key Lab of Nanophotonics and Ultrafine Optoelectronic Systems, School of Physics, Beijing Institute of Technology, Beijing 100081, China;* orcid.org/0000-0001-8441-6027

Yetong Wu − *Centre for Quantum Physics, Key Laboratory of Advanced Optoelectronic Quantum Architecture and Measurement (MOE), School of Physics and Beijing Key Lab of Nanophotonics and Ultrafine Optoelectronic Systems, School of Physics, Beijing Institute of Technology, Beijing 100081, China; Yangtze Delta Region Academy of Beijing Institute of Technology, Jiaxing 314019, China*

Xu Zhang − *Centre for Quantum Physics, Key Laboratory of Advanced Optoelectronic Quantum Architecture and Measurement (MOE), School of Physics and Beijing Key Lab of Nanophotonics and Ultrafine Optoelectronic Systems, School of Physics, Beijing Institute of Technology, Beijing 100081, China; Yangtze Delta Region Academy of Beijing Institute of Technology, Jiaxing 314019, China*

Yongkai Li − *Centre for Quantum Physics, Key Laboratory of Advanced Optoelectronic Quantum Architecture and Measurement (MOE), School of Physics and Beijing Key Lab of Nanophotonics and Ultrafine Optoelectronic Systems, School of Physics, Beijing Institute of Technology, Beijing 100081, China; Yangtze Delta Region Academy of Beijing Institute of Technology, Jiaxing 314019, China*

Tinglu Song − *Experimental Centre of Advanced Materials School of Materials Science & Engineering, Beijing Institute of Technology, Beijing 100081, China*

Wende Xiao − *Centre for Quantum Physics, Key Laboratory of Advanced Optoelectronic Quantum Architecture and Measurement (MOE), School of Physics and Beijing Key Lab of Nanophotonics and Ultrafine Optoelectronic Systems, School of Physics, Beijing Institute of Technology, Beijing 100081, China;* orcid.org/0000-0003-4786-719X

Complete contact information is available at: https://pubs.acs.org/10.1021/acsabm.1c01153

Notes

The authors declare no competing financial interest.

■ ACKNOWLEDGMENTS

This work was supported by the National Key Research and Development Program of China (2020YFA0308800), the National Natural Science Foundation of China (NSFC) (Grants 11734003 and 92065109), the Beijing Natural Science Foundation (Grant Z210006), and the Beijing Institute of Technology (BIT) Research Fund Program for Young Scholars (Grant 3180012222011). We are grateful to the Analysis & Testing Center of the Beijing Institute of Technology for assistance with SEM, STEM, and XRD analyses.

■ REFERENCES

(1) Li, B.; Li, Z.; Situ, B.; Dai, Z.; Liu, Q.; Wang, Q.; Gu, D.; Zheng, L. Sensitive HIV-1 Detection in a Homogeneous Solution Based on an Electrochemical Molecular Beacon Coupled with a Nafion-Graphene Composite Film Modified Screen-Printed Carbon Electrode. *Biosens. Bioelectron.* **2014**, *52*, 330−336.

(2) Kong, H.; Zhang, W.; Yao, J.; Li, C.; Lu, R.; Guo, Z.; Li, J.; Li, C.; Li, Y.; Zhang, C.; Zhou, L. A RT-LAMP Based Hydrogen Ion Selective Electrode Sensing for Effective Detection HIV-1 RNA with High-Sensitivity. *Sens. Actuators, B* **2021**, *329*, 129118.

(3) Yin, D.; Tao, Y.; Tang, L.; Li, W.; Zhang, Z.; Li, J.; Xie, G. Cascade Toehold-Mediated Strand Displacement Along with Non-Enzymatic Target Recycling Amplification for the Electrochemical Determination of the HIV-1 Related Gene. *Microchim. Acta* **2017**, *184*, 3721−3728.

(4) Zou, L.; Shen, R.; Ling, L.; Li, G. Sensitive DNA Detection by Polymerase Chain Reaction with Gold Nanoparticles. *Anal. Chim. Acta* **2018**, *1038*, 105−111.

(5) Yamashige, R.; Kimoto, M.; Okumura, R.; Hirao, I. Visual Detection of Amplified DNA by Polymerase Chain Reaction Using a Genetic Alphabet Expansion System. *J. Am. Chem. Soc.* **2018**, *140*, 14038−14041.

(6) Kang, B.-H.; Lee, Y.; Yu, E.-S.; Na, H.; Kang, M.; Huh, H. J.; Jeong, K.-H. Ultrafast and Real-Time Nanoplasmonic On-Chip Polymerase Chain Reaction for Rapid and Quantitative Molecular Diagnostics. *ACS Nano* **2021**, *15*, 10194−10202.

(7) Koebley, S. R.; Mikheikin, A.; Leslie, K.; Guest, D.; McConnell-Wells, W.; Lehman, J. H.; Juhaishi, T. A.; Zhang, X.; Roberts, C. H.; Picco, L.; Toor, A.; Chesney, A.; Reed, J. Digital Polymerase Chain Reaction Paired with High-Speed Atomic Force Microscopy for Quantitation and Length Analysis of DNA Length Polymorphisms. *ACS Nano* **2020**, *14*, 15385−15393.

(8) Heck, C.; Michaeli, Y.; Bald, I.; Ebenstein, Y. Analytical Epigenetics: Single-Molecule Optical Detection of DNA and Histone Modifications. *Curr. Opin. Biotechnol.* **2019**, *55*, 151−158.

(9) Reyes, J. B.; Kuimova, M. K.; Vilar, R. Metal Complexes as Optical Probes for DNA Sensing and Imaging. *Curr. Opin. Chem. Biol.* **2021**, *61*, 179−190.

(10) Wei, Y.; Huang, Q.; Tian, X.; Zhang, M.; He, J.; Chen, X.; Chen, C.; Deng, Z.; Li, Z.; Chen, S.; Wang, L. Single-Molecule Optical Mapping of the Distribution of DNA Phosphorothioate Epigenetics. *Nucleic Acids Res.* **2021**, *49*, 3672−3680.

(11) Gong, Q.; Yang, H.; Dong, Y.; Zhang, W. A Sensitive Impedimetric DNA Biosensor for the Determination of the HIV Gene Based on Electrochemically Reduced Graphene Oxide. *Anal. Methods* **2015**, *7*, 2554−2562.

(12) Xu, Z.; Yin, K.; Ding, X.; Li, Z.; Sun, X.; Li, B.; Lalla, R. V.; Gross, R.; Liu, C. An Integrated E-Tube Cap for Sample Preparation, Isothermal Amplification and Label-Free Electrochemical Detection of DNA. *Biosens. Bioelectron.* **2021**, *186*, 113306.

(13) Ichzan, A. M.; Hwang, S.-H.; Cho, H.; Fang, C. S.; Park, S.; Kim, G.; Kim, J.; Nandhakumar, P.; Yu, B.; Jon, S.; Kim, K.-s.; Yang, H. Solid-Phase Recombinase Polymerase Amplification Using an Extremely Low Concentration of a Solution Primer for Sensitive Electrochemical Detection of Hepatitis B Viral DNA. *Biosens. Bioelectron.* **2021**, *179*, 113065.
(14) Zamani, M.; Robson, J. M.; Fan, A.; Bono, M. S., Jr.; Furst, A. L.; Klapperich, C. M. Electrochemical Strategy for Low-Cost Viral Detection. *ACS Cent. Sci.* **2021**, *7*, 963−972.
(15) Cui, A.; Zhang, J.; Bai, W.; Sun, H.; Bao, L.; Ma, F.; Li, Y. Signal-on Electrogenerated Chemiluminescence Biosensor for Ultrasensitive Detection of MicroRNA-21 Based on Isothermal Strand-Displacement Polymerase Reaction and Bridge DNA-Gold Nanoparticles. *Biosens. Bioelectron.* **2019**, *144*, 111664.
(16) Wang, H.; Liu, M.; Bai, W.; Sun, H.; Li, Y.; Deng, H. A Convenient Electrogenerated Chemiluminescence Biosensing Method for Selective Detection of 5-Hydroxymethylcytosine in Genomic DNA. *Sens. Actuators, B* **2019**, *284*, 236−242.
(17) Meng, Y.; Bai, W.; Zhang, Y.; Sun, H.; Li, Y. Electrogenerated Chemiluminescence Biosensing Method Based on 5-Hydroxymethylcytosine Antibody and PDDA-CNTs Nanocomposites for the Determination of 5-Hydroxymethylcytosine Double-Stranded DNA. *Talanta* **2020**, *210*, 120597.
(18) Shamsipur, M.; Samandari, L.; Farzin, L.; Besharati-Seidani, A. Development of an Ultrasensitive Electrochemical Genosensor for Detection of HIV-1 Pol Gene Using a Gold Nanoparticles Coated Carbon Paste Electrode Impregnated with Lead Ion-Imprinted Polymer Nanomaterials as a Novel Electrochemical Probe. *Microchem. J.* **2021**, *160*, 105714.
(19) Ye, Y.; Xie, J.; Ye, Y.; Cao, X.; Zheng, H.; Xu, X.; Zhang, Q. A Label-Free Electrochemical DNA Biosensor Based on Thionine Functionalized Reduced Graphene Oxide. *Carbon* **2018**, *129*, 730−737.
(20) Luo, L. Q.; Zhang, Z.; Ding, Y. P.; Deng, D. M.; Zhu, X. L.; Wang, Z. X. Label-Free Electrochemical Impedance Genosensor Based on 1-Aminopyrene/Graphene Hybrids. *Nanoscale* **2013**, *5*, 5833−5840.
(21) Huang, Q.; Lin, X.; Zhu, J.-J.; Tong, Q.-X. Pd-Au@Carbon Dots Nanocomposite: Facile Synthesis and Application as an Ultrasensitive Electrochemical Biosensor for Determination of Colitoxin DNA in Human Serum. *Biosens. Bioelectron.* **2017**, *94*, 507−512.
(22) Blair, E. O.; Corrigan, D. K. A Review of Microfabricated Electrochemical Biosensors for DNA Detection. *Biosens. Bioelectron.* **2019**, *134*, 57−67.
(23) Saheb, A.; Patterson, S.; Josowicz, M. Probing for DNA Methylation with a Voltammetric DNA Detector. *Analyst* **2014**, *139*, 786−792.
(24) Hai, X.; Li, Y.; Zhu, C.; Song, W.; Cao, J.; Bi, S. DNA-Based Label-Free Electrochemical Biosensors: From Principles to Applications. *TrAC, Trends Anal. Chem.* **2020**, *133*, 116098.
(25) Faria, H. A. M.; Zucolotto, V. Label-Free Electrochemical DNA Biosensor for Zika Virus Identification. *Biosens. Bioelectron.* **2019**, *131*, 149−155.
(26) Untiveros, K. L.; Silva, E. G.; Abreu, F. C.; Silva-Júnior, E. F.; Araújo-Junior, J. X.; de Aquino, T. M.; Armas, S. M.; Moura, R. O.; Mendonça-Junior, F. J. B.; Serafim, V. L.; Chumbimuni-Torres, K. An Electrochemical Biosensor Based on Hairpin-DNA Modified Gold Electrode for Detection of DNA Damage by a Hybrid Cancer Drug Intercalation. *Biosens. Bioelectron.* **2019**, *133*, 160−168.
(27) Yu, Y.; Nyein, H. Y. Y.; Gao, W.; Javey, A. Flexible Electrochemical Bioelectronics: The Rise of in Situ Bioanalysis. *Adv. Mater.* **2020**, *32*, 1902083.
(28) Yuan, Y.; Hu, T.; Zhong, X.; Zhu, M.; Chai, Y.; Yuan, R. Highly Sensitive Photoelectrochemical Biosensor Based on Quantum Dots Sensitizing Bi_2Te_3 Nanosheets and DNA-Amplifying Strategies. *ACS Appl. Mater. Interfaces* **2020**, *12*, 22624−22629.
(29) Novelli, P.; Taddei, F.; Geim, A. K.; Polini, M. Failure of Conductance Quantization in Two-Dimensional Topological Insulators due to Nonmagnetic Impurities. *Phys. Rev. Lett.* **2019**, *122*, No. 016601.
(30) Deng, M. X.; Ma, R.; Luo, W.; Shen, R.; Sheng, L.; Xing, D. Y. Time-Reversal Invariant Resonant Backscattering on a Topological Insulator Surface Driven by a Time-Periodic Gate Voltage. *Sci. Rep.* **2018**, *8*, 12338.
(31) Zhang, P.; Noguchi, R.; Kuroda, K.; Lin, C.; Kawaguchi, K.; Yaji, K.; Harasawa, A.; Lippmaa, M.; Nie, S.; Weng, H.; Kandyba, V.; Giampietri, A.; Barinov, A.; Li, Q.; Gu, G. D.; Shin, S.; Kondo, T. Observation and Control of the Weak Topological Insulator State in $ZrTe_5$. *Nat. Commun.* **2021**, *12*, 406.
(32) Gao, S. Y.; Xu, S.; Li, H.; Yi, C. J.; Nie, S.-M.; Rao, Z. C.; Wang, H.; Hu, Q. X.; Chen, X. Z.; Fan, W. H.; Huang, J. R.; Huang, Y. B.; Pryds, N.; Shi, M.; Wang, Z. J.; Shi, Y. G.; Xia, T. L.; Qian, T.; Ding, H. Time-Reversal Symmetry Breaking Driven Topological Phase Transition in EuB_6. *Phys. Rev. X* **2021**, *11*, No. 021016.
(33) Hossain, M. Z.; Rumyantsev, S. L.; Teweldebrhan, D.; Shahil, K. M. F.; Shur, M.; Balandin, A. A. 1/f Noise in Conducting Channels of Topological Insulator Materials. *Phys. Status Solidi A* **2011**, *208*, 144−146.
(34) Ding, J.; Liu, C.; Zhang, Y.; Kalappattil, V.; Yu, R.; Erugu, U.; Tang, J.; Ding, H.; Chen, H.; Wu, M. Large Damping Enhancement in Dirac-Semimetal−Ferromagnetic-Metal Layered Structures Caused by Topological Surface States. *Adv. Funct. Mater.* **2021**, *31*, 2008411.
(35) Rechciński, R.; Galicka, M.; Simma, M.; Volobuev, V. V.; Caha, O.; Sánchez-Barriga, J.; Mandal, P. S.; Golias, E.; Varykhalov, A.; Rader, O.; Bauer, G.; Kacman, P.; Buczko, R.; Springholz, G. Structure Inversion Asymmetry and Rashba Effect in Quantum Confined Topological Crystalline Insulator Heterostructures. *Adv. Funct. Mater.* **2021**, *31*, 2008885.
(36) Ando, Y. Topological Insulator Materials. *J. Phys. Soc. Jpn.* **2013**, *82*, 102001.
(37) Yang, C.; Cattelan, M.; Fox, N.; Huang, Y.; Golden, M. S.; Schwarzacher, W. Electrochemical Modification and Characterization of Topological Insulator Single Crystals. *Langmuir* **2019**, *35*, 2983−2988.
(38) Chiatti, O.; Riha, C.; Lawrenz, D.; Busch, M.; Dusari, S.; Sánchez-Barriga, J.; Mogilatenko, A.; Yashina, L. V.; Valencia, S.; Ünal, A. A.; Rader, O.; Fischer, S. F. 2D Layered Transport Properties from Topological Insulator Bi_2Se_3 Single Crystals and Micro Flakes. *Sci. Rep.* **2016**, *6*, 27483.
(39) Yildiz, D.; Kisiel, M.; Gysin, U.; Gürlü, O.; Meyer, E. Mechanical Dissipation via Image Potential States on a Topological Insulator Surface. *Nat. Mater.* **2019**, *18*, 1201−1206.
(40) Wu, S.; Liu, G.; Li, P.; Liu, H.; Xu, H. A High-Sensitive and Fast-Fabricated Glucose Biosensor Based on Prussian Blue/Topological Insulator Bi_2Se_3 Hybrid Film. *Biosens. Bioelectron.* **2012**, *38*, 289−294.
(41) Chen, S.; Fang, Y. M.; Li, J.; Sun, J. J.; Chen, G. N.; Yang, H. H. Study on the Electrochemical Catalytic Properties of the Topological Insulator Bi_2Se_3. *Biosens. Bioelectron.* **2013**, *46*, 171−174.
(42) Xiao, L.; Zhu, A.; Xu, Q.; Chen, Y.; Xu, J.; Weng, J. Colorimetric Biosensor for Detection of Cancer Biomarker by Au Nanoparticle-Decorated Bi_2Se_3 Nanosheets. *ACS Appl. Mater. Interfaces* **2017**, *9*, 6931−6940.
(43) Mohammadniaei, M.; Yoon, J.; Lee, T.; Bharate, B. G.; Jo, J.; Lee, D.; Choi, J.-W. Electrochemical Biosensor Composed of Silver Ion-Mediated dsDNA on Au-Encapsulated Bi_2Se_3 Nanoparticles for the Detection of H_2O_2 Released from Breast Cancer Cells. *Small* **2018**, *14*, 1703970.
(44) Arakane, T.; sato, T.; souma, S.; Kosaka, K.; Nakayama, K.; Komatsu, M.; Takahashi, T.; Ren, Z.; segawa, K.; Ando, Y. Tunable Dirac Cone in the Topological Insulator $Bi_{2-x}Sb_xTe_{3-y}Se_y$. *Nat. Commun.* **2012**, *3*, 636.
(45) Tu, N. H.; Tanabe, Y.; Huynh, K. K.; Sato, Y.; Oguro, H.; Heguri, S.; Tsuda, K.; Terauchi, M.; Watanabe, K.; Tanigaki, K. Van der Waals epitaxial growth of topological insulator $Bi_{2-x}Sb_xTe_{3-y}Se_y$ ultrathin nanoplate on electrically insulating fluorophlogopite mica. *Appl. Phys. Lett.* **2014**, *105*, No. 063104.

https://doi.org/10.1021/acsabm.1c01153
ACS Appl. Bio Mater. 2022, 5, 1084−1091

(46) Sulaev, A.; Zeng, M.; Shen, S.-Q.; Cho, S. K.; Zhu, W. G.; Feng, Y. P.; Eremeev, S. V.; Kawazoe, Y.; Shen, L.; Wang, L. Electrically Tunable in-Plane Anisotropic Magnetoresistance in Topological Insulator $BiSbTeSe_2$ Nanodevices. *Nano Lett.* **2015**, *15*, 2061−2066.
(47) Hsiung, T.-C.; Mou, C.-Y.; Lee, T.-K.; Chen, Y.-Y. Surface-Dominated Transport and Enhanced Thermoelectric Figure of Merit in Topological Insulator $Bi_{1.5}Sb_{0.5}Te_{1.7}Se_{1.3}$. *Nanoscale* **2015**, *7*, 518−523.
(48) Xu, Y.; Miotkowski, I.; Liu, C.; Tian, J.; Nam, H.; Alidoust, N.; Hu, J.; Shih, C.-K.; Hasan, M. Z.; Chen, Y. P. Observation of Topological Surface State Quantum Hall Effect in an Intrinsic Three-Dimensional Topological Insulator. *Nat. Phys.* **2014**, *10*, 956−963.
(49) Han, K.-B.; Chong, S. K.; Oliynyk, A. O.; Nagaoka, A.; Petryk, S.; Scarpulla, M. A.; Deshpande, V. V.; Sparks, T. D. Enhancement in Surface Mobility and Quantum Transport of $Bi_{2-x}Sb_xTe_{3-y}Se_y$ Topological Insulator by Controlling the Crystal Growth Conditions. *Sci. Rep.* **2018**, *8*, 17290.
(50) Li, S.-S.; Hu, Y.-Y.; Wang, A.-J.; Weng, X.; Chen, J.-R.; Feng, J.-J. Simple Synthesis of Worm-Like Au−Pd Nanostructures Supported on Reduced Graphene Oxide for Highly Sensitive Detection of Nitrite. *Sens. Actuators, B* **2015**, *208*, 468−474.
(51) Huang, Q.; Lin, X.; Lin, C.; Zhang, Y.; Zhang, H.; Hu, S.; Wei, C.; Tong, Q.-X. Ultrasensitive-Electrochemical Sensor for the Detection of Luteolin in Chrysanthemums and Peanut Shells Using an Au/Pd/Reduced Graphene Oxide Nanofilm. *Anal. Methods* **2016**, *8*, 6347−6352.
(52) Shajaripour Jaberi, S. Y.; Ghaffarinejad, A.; Omidinia, E. An Electrochemical Paper Based Nano-Genosensor Modified with Reduced Graphene Oxide-Gold Nanostructure for Determination of Glycated Hemoglobin in Blood. *Anal. Chim. Acta* **2019**, *1078*, 42−52.
(53) Lu, Q.; Su, T.; Shang, Z.; Jin, D.; Shu, Y.; Xu, Q.; Hu, X. Flexible Paper-Based Ni-MOF Composite/AuNPs/CNTs Film Electrode for HIV DNA Detection. *Biosens. Bioelectron.* **2021**, *184*, 113229.
(54) Nagar, B.; Balsells, M.; la Escosura-Muñiz, A.; Gomez-Romero, P.; Merkoçi, A. Fully Printed One-Step Biosensing Device Using Graphene/AuNPs Composite. *Biosens. Bioelectron.* **2019**, *129*, 238−244.
(55) Wang, C.; Li, Y.; Zhao, Q. A Signal-on Electrochemical Aptasensor for Rapid Detection of Aflatoxin B1 Based on Competition with Complementary DNA. *Biosens. Bioelectron.* **2019**, *144*, 111641.
(56) Zhao, K. R.; Wang, L.; Liu, P. F.; Hang, X. M.; Wang, H. Y.; Ye, S. Y.; Liu, Z. J.; Liang, G. X. A Signal-Switchable Electrochemiluminescence Biosensor Based on the Integration of Spherical Nucleic Acid and CRISPR/Cas12a for Multiplex Detection of HIV/HPV DNAs. *Sens. Actuators, B* **2021**, *346*, 130485.
(57) Cai, Q.; Wu, D.; Li, H.; Jie, G.; Zhou, H. Versatile Photoelectrochemical and Electrochemiluminescence Biosensor Based on 3D CdSe QDs-DNA Nanonetwork-SnO_2 Nanoflower Coupled with DNA Walker Amplification for HIV Detection. *Biosens. Bioelectron.* **2021**, *191*, 113455.

https://doi.org/10.1021/acsabm.1c01153
ACS Appl. Bio Mater. 2022, 5, 1084−1091